Image-Reject Mixer With Large Suppression of Mixing Spurs Based on a Photonic Microwave Phase Shifter

Zhenzhou Tang, *Student Member, IEEE*, and Shilong Pan, *Senior Member, IEEE*

***Abstract*—Image-reject mixers (IRMs) play an important role in microwave and millimeter-wave receivers to eliminate the interference from the image frequency. The keys to realizing a wideband IRM are the precise 90° phase shifting and parallel frequency mixing within a large operational frequency range. In this paper, we propose and demonstrate a novel photonic scheme that can perform simultaneously wideband 90° phase shifting and parallel frequency mixing based on a dual-polarization dual-drive Mach–Zehnder modulator and an optical filter. An IRM is thus implemented. A proof-of-concept experiment is carried out. The experimental results show that the image rejection ratio of the proposed IRM reaches ∼60 dB, when the RF and LO frequencies are tuned in a frequency range of 10–40 GHz. In addition, since the optical filter is employed to select only the two +first-order RF and LO sidebands, the unwanted mixing spurs are all suppressed below the noise floor.**

***Index Terms*—I/Q mixer, image reject mixer, mixer, microwave photonics, phase shifter.**

I. Introduction

THE frequency downconverter is one of the most important components of today's microwave and millimeter-wave receiver, through which an RF signal with a frequency of ω_{RF} is multiplied with a local oscillator (LO) signal at a frequency of ω_{LO} to produce an intermediate frequency (IF) signal at $\omega_{\mathrm{IF}} = \omega_{\mathrm{RF}} - \omega_{\mathrm{LO}}$. Although the frequency downconversion has been performed in the electrical domain for decades, photonic microwave downconverters have recently garnered significant interest from researchers and developers due to the advantages offered by the photonic technologies in terms of large bandwidth, high isolation, and immunity to electromagnetic interference [1]–[9].

Previously, the most common method to perform photonic microwave mixing has been based on the external modulation by two cascaded intensity modulators [1]. The principle is that when an optical carrier is modulated by the RF and LO signals in series, various RF and LO sidebands around the optical carrier would be produced. Due to the frequency-beating between the first-order RF and LO sidebands at a photodetector (PD), the downconverted IF signal could be obtained. Although this photonic microwave mixer has the advantage of very high isolation between the RF and LO ports, it can only achieve the simplest single-ended mixing, facing problems such as poor image rejection and mixing spur suppression.

The image is the input noise or interference signal at the frequency of $\omega_{\mathrm{IM}} = \omega_{\mathrm{LO}} - \omega_{\mathrm{IF}}$. If the image is sent to the frequency downconverter together with the useful RF signal, an unwanted frequency component with a frequency of $\omega_{\mathrm{IF}'} = \omega_{\mathrm{LO}} - \omega_{\mathrm{IM}}$ is generated. Since $\omega_{\mathrm{IF}'}$ is identical to ω_{IF}, the undesirable signal downconverted from the image cannot be separated through electrical filtering.

To realize the image rejection, a quite straight-forward way is pre-filtering of the input electrical or optical signal using an electrical filter [10] or an optical filter [11]. Similar to the filter-based methods employed in the pure-electrical image-reject mixer (IRM), this kind of method cannot support wide bandwidth operation. In addition, because the slope of the filter must be sharp enough to suppress the image without affecting the wanted signal, the method cannot work when the IF frequency is very low.

The phase cancellation method [12], [13], e.g., the Hartley method, is another effective scheme to realize image rejection mixing. The basic idea of this method is to obtain a pair of quadrature IF outputs by introducing a pair of quadrature LO signals to two parallel single-ended frequency mixers. When using an electrical quadrature hybrid coupler to combine the two IF outputs, the image would be suppressed because the two unwanted IF signals downconverted from the image are out of phase while the desired components are in phase [14]. The key component in the phase-cancellation-method based IRM is the electrical quadrature hybrid for generation of the quadrature LO signals, which must be operated in the RF band. The state-of-the-art electrical quadrature hybrid, however, cannot produce a precise 90° phase difference across a wide frequency range (especially in the high-frequency regime), resulting in a small operational bandwidth or a low image rejection ratio of the IRM.

The mixing spurs are located at the frequencies of $n\omega_{\mathrm{RF}} \pm m\omega_{\mathrm{LO}}$, which are generated by the nonlinearity of the mixer. The existence of the mixing spurs would restrict the operational bandwidth of the designed frequency mixer, since the input signal should be restricted to a relatively narrow frequency range to avoid the output frequency aliasing. Mixing

Manuscript received January 16, 2016; revised March 8, 2016; accepted March 27, 2016. Date of publication April 3, 2016; date of current version September 25, 2016. This work was supported in part by the National Basic Research Program of China under Grant 2012CB315705, in part the National Natural Science Foundation of China under Grants 61422108 and 61527820, in part by the Fundamental Research Funds for the Central Universities, and in part by a Project Funded by the Priority Academic Program Development of Jiangsu Higher Education Institutions.

The authors are with the Key Laboratory of Radar Imaging and Microwave Photonics, Nanjing University of Aeronautics and Astronautics, Ministry of Education, Nanjing 210016, China (e-mail: pans@ieee.org).

Color versions of one or more of the figures in this paper are available online at http://ieeexplore.ieee.org.

Digital Object Identifier 10.1109/JLT.2016.2550180

spur suppression is usually implemented by removing the useless optical components before photodetection [15]. For example, the carrier-suppression modulation in [16] efficiently suppressed the carrier-related mixing spurs, especially the RF and LO leakages. By suppressing one of the first-order sidebands, the sideband spurs can be further reduced [17]. Parallel optical filtering, which select only the two +first- or −first-order RF and LO sidebands, is another effective way to suppress mixing spurs [18], but two electro-optic modulators and two narrowband optical filters are required, leading to a complex and bulky system. Moreover, it should be noted that most of the existing photonic microwave mixers can achieve either image rejection or mixing-spur suppression, but not both. Recently, we proposed a reconfigurable photonic microwave mixer which can realize simultaneously image rejection and mixing-spur suppression [19]. However, like the mixers demonstrated in [18], parallel modulations, filtering, and amplifications are required.

In this paper, a novel photonic microwave IRM using a dual-polarization dual-drive Mach–Zehnder modulator (DPol-DMZM) and an optical bandpass filter (OBPF) is proposed and demonstrated. Each sub-DMZM can perform single-ended mixing [16], and the sub-DMZM together with the OBPF realizes a photonic microwave phase shifter. By adjusting the phase shift via tuning the bias voltage of the sub-DMZM [20], a precise 90° optical phase shift is introduced between the two parallel single-ended mixers formed by the two sub-DMZMs. With a low-frequency electrical quadrature hybrid coupler to combine the IF outputs of the two single-ended mixers, a phase-cancellation-based IRM is realized. In addition, the OBPF in the photonic microwave phase shifter can remove most of the undesirable sidebands, leading to large suppression of the mixing spurs. A numerical analysis and a proof-of-concept experiment are conducted. The measured results show that the image-rejection ratio is ∼60 dB when the RF/LO frequency is tuned in a frequency range of 10–40 GHz. Besides, only the useful IF signal is obtained at the output of the proposed IRM, and all the mixing spurs are suppressed below the noise floor. Compared to the photonic IRMs [10]–[13] demonstrated before, a significant improvement of the proposed approach is that no high-frequency electrical 90° hybrid is necessary thanks to the wideband photonic method for achieving a microwave phase shift [20]. In addition, since only a single electro-optic modulator is used for parallel modulation, an OBPF and an optical amplifier are enough for the filtering and amplification of both the RF and LO sidebands, resulting in a much simpler structure than those in [12], [13], [18], [19].

II. Principle

A. System Structure

Fig. 1 shows the schematic diagram of the proposed photonic IRM. An optical carrier from a laser diode (LD) is sent to a DPol-DMZM via a polarization controller (PC, PC1). The DPol-DMZM is an integrated device which consists of a polarization beam splitter (PBS), two sub-DMZMs (DMZM1 and DMZM2), and a polarization beam combiner (PBC). The detailed structure is shown in the dashed box in Fig. 1. In the

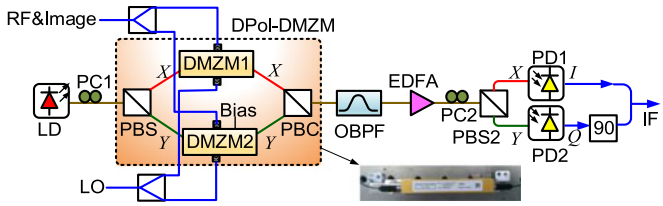

Fig. 1. Schematic diagram of the proposed photonic IRM. LD: laser diode; PC: polarization controller; DPol-DMZM: dual-polarization dual-drive Mach-Zehnder modulator; OBPF: optical bandpass filter; EDFA: erbium-doped fiber amplifier; PD: photodetector; PBS: polarization beam splitter; PBC: polarization beam combiner. Inset: photograph of the DPol-DMZM.

DPol-DMZM, the optical carrier is first split into two orthogonal branches (*X*- and *Y*-polarizations) by the PBS, then sent to the two respective sub-DMZMs. The received signal (including the useful RF signal and useless image) is split into two equal parts and introduced to one of the respective RF ports of DMZM1 and DMZM2. At the same time, an LO signal is split into two equal portions and applied to the other respective RF ports of DMZM1 and DMZM2. The optical signals from the two orthogonal branches are then combined by the PBC, and sent to an OBPF, by which the +first-order RF and LO sidebands are selected. An erbium-doped fiber amplifier (EDFA) is inserted to compensate the system loss. The amplified signal is sent to PC2 and PBS2, which is demultiplexed into two orthogonal portions and detected by two PDs (PD1 and PD2). When adjusting the bias voltage applied to one of the sub-MZMs, e.g., DMZM2 in Fig. 1, a 90° phase shift would be introduced to the IF signal obtained by PD2 [20]. In this way, the output IF signals of the two PDs can be in quadrature. As a result, a photonic microwave I/Q mixer is obtained. To realize image-reject mixing, a low-frequency electrical 90° hybrid at the IF-band is employed to combine the two quadrature outputs of the I/Q mixer.

B. DMZM-Based Single-Ended Frequency Mixer

Taking use of polarization multiplexing in the DPol-DMZM and polarization demultiplexing by PC2 and PBS2, the proposed mixer can be viewed as two parallel single-ended frequency mixers based on DMZMs [16]. Each frequency mixer contains the LD, a sub-DMZM, the OBPF, the EDFA and a PD. If the difference between the unmodulated phases in the two arms of the DMZM is zero, the output optical signal of the DMZM is given by

$$E_x = \frac{\sqrt{P_{\rm in}}}{2}\sqrt{t_{\rm M}}\exp\left(j\omega_c t\right)\cdot\left[\exp\left(j\beta_{\rm RF}\cos\left(\omega_{\rm RF}t\right)\right) + \exp\left(j\beta_{\rm LO}\cos\left(\omega_{\rm LO}t\right)\right)\right] \quad (1)$$

where $\omega_{\rm c}$, $\omega_{\rm RF}$ and $\omega_{\rm LO}$ are the angular frequencies of the optical carrier, RF and LO signals, respectively, $P_{\rm in}$ is the input power of the optical carrier, $t_{\rm M}$ is the insertion loss of the DMZM, $\beta_{\rm RF}$ and $\beta_{\rm LO}$ are the modulation indexes at the two arms of the DMZM. Under small signal modulation, (1) can be

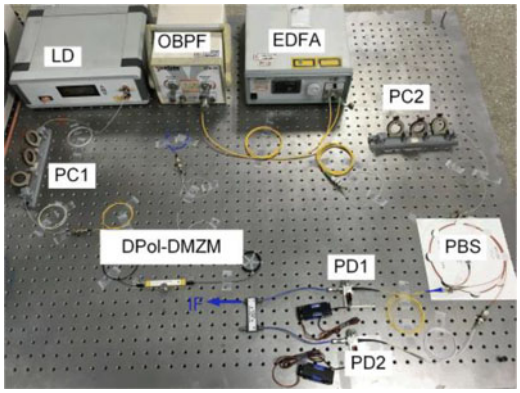

Fig. 2. Photograph of the experiment setup of the proposed IRM.

expanded as

$$E_x = \frac{\sqrt{P_{\rm in}}}{2}\sqrt{t_{\rm M}}\left\{\left[J_0\left(\beta_{\rm RF}\right)+J_0\left(\beta_{\rm LO}\right)\right]\exp\left(j\omega_c t\right)\right.$$
$$+\left[jJ_1\left(\beta_{\rm RF}\right)\exp\left(j\left(\omega_c-\omega_{\rm RF}\right)t\right)+jJ_1\left(\beta_{\rm RF}\right)\right.$$
$$\left.\exp\left(j\left(\omega_c+\omega_{\rm RF}\right)t\right)\right]$$
$$+\left[jJ_1\left(\beta_{\rm LO}\right)\exp\left(j\left(\omega_c-\omega_{\rm LO}\right)t\right)+jJ_1\left(\beta_{\rm LO}\right)\right.$$
$$\left.\left.\exp\left(j\left(\omega_c+\omega_{\rm LO}\right)t\right)\right]\right\}. \quad (2)$$

Through the OBPF, only the two +first-order sidebands are selected, we obtain

$$E_x = \frac{\sqrt{P_{\rm in}}}{2}\sqrt{t_{\rm M}t_{\rm F}}\left[jJ_1\left(\beta_{\rm RF}\right)\exp\left(j\left(\omega_c+\omega_{\rm RF}\right)t\right)\right.$$
$$\left.+jJ_1\left(\beta_{\rm LO}\right)\exp\left(j\left(\omega_c+\omega_{\rm LO}\right)t\right)\right] \quad (3)$$

where $t_{\rm F}$ is the insertion loss of the OBPF. When the optical signal in (3) is amplified by the EDFA and detected by the PD, the obtained ac term of the detected photocurrent is given by

$$i_x=\frac{P_{\rm in}}{2}\Re t_{\rm M}t_{\rm F}G\cdot J_1\left(\beta_{\rm RF}\right)J_1\left(\beta_{\rm LO}\right)\cos\left[\left(\omega_{\rm RF}-\omega_{\rm LO}\right)t\right] \quad (4)$$

where G is the gain of the EDFA and $\Re$ is the responsivity of the PD. From (4), the downconverted IF signal is obtained at the output of the PD. Besides, since only the two +first-order sidebands are applied to the PD, the unwanted mixing spurs are significantly suppressed.

C. Photonic Microwave Phase Shifter

The bias voltage of the sub-DMZM can be adjusted to tune the phase of the downconverted signal. If there is a phase difference between the two arms of the DMZM, (3) can be rewritten as

$$E_y = \frac{\sqrt{P_{\rm in}}}{2}\sqrt{t_{\rm M}t_{\rm F}}\left[jJ_1\left(\beta_{\rm RF}\right)\exp\left(j\left(\omega_c+\omega_{\rm RF}\right)t\right)\right.$$
$$\left.+jJ_1\left(\beta_{\rm LO}\right)\exp\left(j\left(\omega_c+\omega_{\rm LO}\right)t+j\phi\right)\right] \quad (5)$$

where $\phi=\pi V_{\rm bias}/V_\pi$ is the phase difference between the two arms of the DMZM, $V_{\rm bias}$ is the bias voltage and V_π is the half-wave voltage of the DMZM. After optical amplification by the EDFA and photodetection by the PD, the obtained ac term of the detected photocurrent is given by

$$i_y = \frac{P_{\rm in}}{2}\Re t_{\rm M}t_{\rm F}G\cdot J_1\left(\beta_{\rm RF}\right)J_1\left(\beta_{\rm LO}\right)\cos\left[\left(\omega_{\rm RF}-\omega_{\rm LO}\right)t-\phi\right]. \quad (6)$$

Compared to the signal in (4), the optical phase difference introduced by the bias voltage in (5) is mapped to the microwave phase shift of the frequency-downconverted IF signal.

D. Image-Reject Mixing

According to the principle of the Hartley method [14], to realize the image rejection, the bias voltage applied to one of the two sub-DMZMs (DMZM2 for example) in the DPol-DMZM is adjusted to let $\phi=\pi/2$. When the useful RF signal and the unwanted image are both applied to the proposed IRM, the outputs of PD1 and PD2 are

$$\begin{bmatrix} i_x \\ i_y \end{bmatrix} = \frac{P_{\rm in}}{2}\Re t_{\rm M}t_{\rm F}G$$
$$\cdot\begin{bmatrix} J_1\left(\beta_{\rm RF}\right)J_0\left(\beta_{\rm IM}\right)J_1\left(\beta_{\rm LO}\right)\cos\left[\left(\omega_{\rm RF}-\omega_{\rm LO}\right)t\right] \\ +J_1\left(\beta_{\rm IM}\right)J_0\left(\beta_{\rm RF}\right)J_1\left(\beta_{\rm LO}\right)\cos\left[\left(\omega_{\rm LO}-\omega_{\rm IM}\right)t\right] \\ J_1\left(\beta_{\rm RF}\right)J_0\left(\beta_{\rm IM}\right)J_1\left(\beta_{\rm LO}\right)\sin\left[\left(\omega_{\rm RF}-\omega_{\rm LO}\right)t\right] \\ -J_1\left(\beta_{\rm IM}\right)J_0\left(\beta_{\rm RF}\right)J_1\left(\beta_{\rm LO}\right)\sin\left[\left(\omega_{\rm LO}-\omega_{\rm IM}\right)t\right] \end{bmatrix} \quad (7)$$

where $\omega_{\rm RF}$ and $\omega_{\rm IM}$ are the angular frequencies of the useful RF signal and the unwanted image ($\omega_{\rm RF}-\omega_{\rm LO}=\omega_{\rm LO}-\omega_{\rm IM}$) and $\beta_{\rm IM}$ is the modulation index related to the amplitude of the image. As can be seen, the IF signals downconverted from the useful RF signal are quadrature and have the same sign, while the IF signals downconverted from the image are in quadrature but have the opposite signs. If a low-frequency electrical 90° hybrid is employed to combine the two quadrature outputs in Eq. (7), the combined signal can be written as

$$i = \frac{P_{\rm in}}{2}\Re t_{\rm M}t_{\rm F}t_{\rm H}G\cdot$$
$$\left\{J_1\left(\beta_{\rm RF}\right)J_0\left(\beta_{\rm IM}\right)J_1\left(\beta_{\rm LO}\right)\left[\cos\left[\left(\omega_{\rm RF}-\omega_{\rm LO}\right)t\right]\right.\right.$$
$$\left.+\ \sin\left[\left(\omega_{\rm RF}-\omega_{\rm LO}\right)t+\pi/\pi 2\right]\right]$$
$$+J_1\left(\beta_{\rm IM}\right)J_0\left(\beta_{\rm RF}\right)J_1\left(\beta_{\rm LO}\right)\left[\cos\left[\left(\omega_{\rm LO}-\omega_{\rm IM}\right)t\right]\right.$$
$$\left.\left.-\ \sin\left[\left(\omega_{\rm LO}-\omega_{\rm IM}\right)t+\pi/2\right]\right]\right\}$$
$$= P_i\Re t_{\rm M}t_{\rm F}t_{\rm H}G\cdot J_1\left(\beta_{\rm RF}\right)J_0\left(\beta_{\rm IM}\right)J_1\left(\beta_{\rm LO}\right)$$
$$\times\cos\left[\left(\omega_{\rm RF}-\omega_{\rm LO}\right)t\right] \quad (8)$$

where $t_{\rm H}$ is the insertion loss of the electrical 90° hybrid coupler. As can be seen from (8), the IF signal downconverted from the image is suppressed.

Thanks to the wideband photonic microwave phase shifter, no high-frequency electrical 90° hybrid coupler is needed. The phase shift can be adjusted to be precisely 90°, which is almost frequency independent. In addition, the photonic microwave phase shifter in the proposed IRM is voltage-controlled, so a feed-back circuit can guarantee the best possible image-reject performance. Since the optical filter only selects useful sidebands, the mixing spurs can be effectively suppressed. Furthermore, only a single integrated modulator is applied in the

TABLE I
PARAMETERS OF THE MAIN DEVICES IN THE EXPERIMENT SETUP

Symbol	Parameter	Value
P_{in}	input optical power	16 dBm
t_M	insertion loss of the DPol-DMZM	13 dB
t_F	insertion loss of the OBPF	12 dB
$\Re$	PD responsivity	0.65 A/W
G	gain of EDFA	20 dB
$\beta_{RF,IM}$	RF/image modulation index	0.35
β_{LO}	LO modulation index	0.4
R_L	equivalent PD load resistance	50 Ω
t_H	Insertion loss of the electrical hybrid coupler	3 dB

proposed IRM, making it simpler and more compact than other ones [10]–[13], [19].

III. EXPERIMENTAL RESULTS AND DISCUSSES

A proof-of-concept experiment based on the configuration shown in Fig. 1 is carried out. The photograph of the experiment setup of the proposed IRM is shown in Fig. 2, and the main parameters of the devices are listed in Table I. An optical carrier with a wavelength of 1551 nm and a power of 16 dBm is generated by an LD and sent to a DPol-DMZM (Fujitsu FTM7980) via a PC. An RF signal generated by a vector signal generator (Agilent E8267D) and an LO signal produced by an analog signal generator (Agilent E8257D) are both split into two equals by two electrical power splitters, respectively. One part of the RF signal and one part of the LO signal are sent to the RF ports of DMZM1, and the other parts of RF and LO signals are applied to DMZM2. An OBPF (Yenista XTM-50) is used to select the +first-order sidebands. The output signal from the OBPF is polarization demultiplexed by PC2 and PBS2. Then, two identical PDs with bandwidths of 45 GHz and responsivities of 0.65 A/W (u2t 2120RA) are employed for photodetection. The two output signals of PD1 and PD2 are combined by a low-frequency electrical 90° hybrid. The pigtails of the DPol-DMZM and PBS2 are polarization maintaining fibers and others are standard single-mode fibers. The optical spectrum is measured by an optical spectrum analyzer (YOKOGAWA AQ6370C) and the electrical spectrum is observed by a 43-GHz electrical signal analyzer (Agilent N9030A). In addition, a 32-GHz four-channel digital oscilloscope (Agilent DSO-X 92504A) is used to measure the electrical waveforms.

A. Polarization Multiplexing and De-Multiplexing

The theoretical analysis presented in Section II is based on the assumption that the modulated optical signal at the output of the DPol-DMZM can be effectively demultiplexed by PC2 and PBS2 before photodetection. This is of great importance to implement independent parallel modulation by using a single DPol-DMZM. Therefore, in the first step, the performance of polarization multiplexing and demultiplexing is studied. The frequencies of the RF and LO signals are set to be 21 and 20 GHz, respectively. The polarization multiplexing is realized in the DPol-DMZM. Fig. 3 shows the optical spectra of the

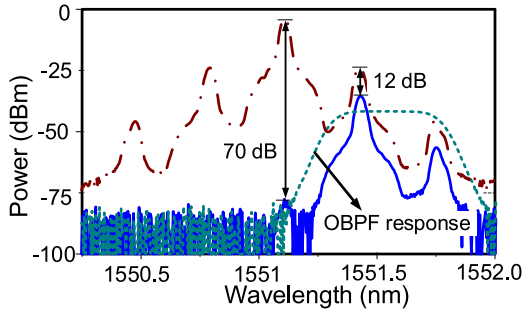

Fig. 3. Optical spectra of the optical signals before (dash-dotted line) and after (solid line) the OBPF. Dashed line: filter response.

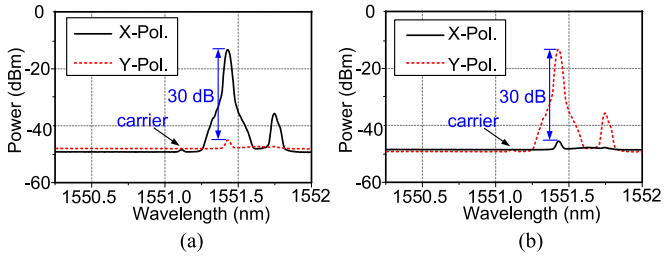

Fig. 4. Optical spectra measured at the outputs of PBS2 when (a) DMZM2 or (b) DMZM1 is undriven.

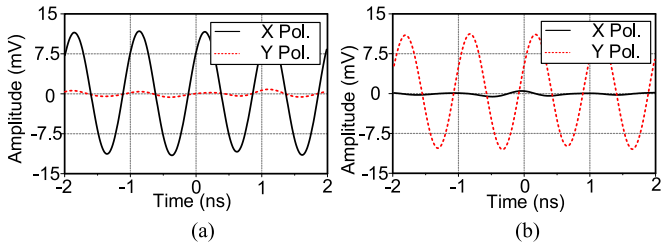

Fig. 5. Electrical waveforms obtained by PD1 and PD2 when (a) DMZM2 or (b) DMZM1 is undriven.

signals before and after the OBPF. The transmission response of the OBPF is also plotted as the dashed line. Due to the high roll-off factor of the OBPF (500 dB/nm), only the positive sidebands are selected and the optical carrier is suppressed by more than 70 dB. After optical amplification by the EDFA, the polarization-multiplexed signal is sent to PC2 and PBS2. Fig. 4(a) shows the optical spectrum when the RF and LO signals are only applied to DMZM1. As can be seen, the *Y*-polarized optical signal is nearly unmodulated, and the power of the optical sidebands are more than 30 dB lower than that of the *X*-polarized optical signal. If the two orthogonal outputs of PBS2 are sent to PD1 and PD2, respectively, the waveforms of the obtained IF signals are shown in Fig. 5(a). As marked by the solid line, the frequency-converted signal is only observed at the output of PD1.

Similarly, when the RF and LO signals are applied to DMZM2 only, the measured optical spectra are presented in Fig. 4(b). As compared with the spectra in Fig. 4(a), the *X*-polarized optical signal is nearly unmodulated, and its power is about 30-dB

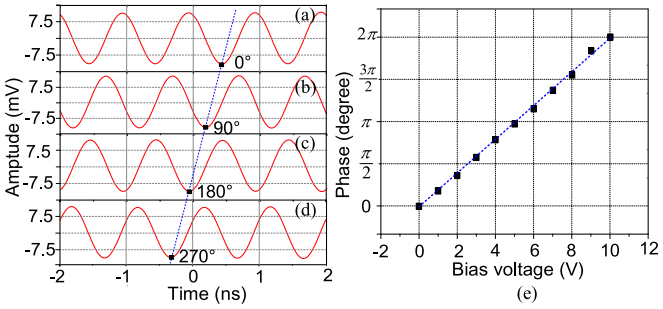

Fig. 6. (a)–(d) Electrical waveforms of the IF signals measured at the output of PD2 with different phase shifts, and (e) the phase shift versus the dc bias voltage applied to DMZM2.

lower than that of the *Y*-polarized signal. Fig. 5(b) shows the corresponding electrical waveforms from the two PDs, indicating again that the optical signal could be efficiently demultiplexed.

B. Photonic Microwave Phase Shifting

The photonic microwave phase shifter is the key component to realize image-reject mixing. As can be seen from the electrical waveforms in Fig. 5(a) and (b), the obtained two IF signals are nearly in phase, if no bias voltage is applied to the sub-DMZMs. To achieve the image rejection, a 90° phase difference should be introduced between the two output IF signals. To do so, in the proposed IRM, the bias voltage of DMZM2 is adjusted to change the phase of the IF signal obtained by PD2. Fig. 6(a)–(d) show the electrical waveforms of the IF signals output from PD2 when the bias voltage applied to DMZM2 is adjusted. As can be seen, a phase shift within 0–360° is successfully introduced to the *Y*-polarized output. The phase shift versus the dc bias voltage applied to DMZM2 is also shown in Fig. 6(e). The phase shift increases linearly with the bias voltage applied to DMZM2 over a full 360° phase tuning range when the bias voltage changes from 0 to 10 V. Therefore, a photonic microwave phase shifter is performed in the proposed IRM. It should be noted that the amplitude of the IF signal keeps unchanged when the phase shift is changed. Meanwhile, since the bias voltage is only applied to DMZM2, only the IF signal obtained by PD2 would be phase shifted and the phase of the IF signal obtained from the *X*-polarized branch keeps unchanged.

C. Image-Reject Mixing With Spurs Suppression

Taking use of the photonic microwave phase shifter, a quadrature phase difference is introduced between the IF signals obtained from the *X*- and *Y*-polarized branches. Fig. 7(a) shows the measured waveforms of the obtained IF signals. As can be seen, a pair of IF signals with same amplitude and quadrature phase shift are obtained. When the two IF signals are combined by the low-frequency electrical 90° hybrid, the waveform of the combined signal is shown in Fig. 7(b). When the frequency of the RF signal is changed to the image frequency (i.e., 19 GHz), the waveforms of the two IF signals from the two PDs are shown in Fig. 8(a). As compared with the waveforms in Fig. 7(a), although the two signals are still in quadrature, the IF signal

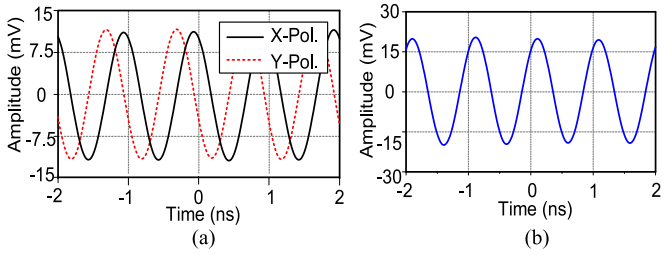

Fig. 7. Waveforms of the IF signals output from (a) PD1 and PD2, and (b) the proposed IRM when the useful RF signal is applied.

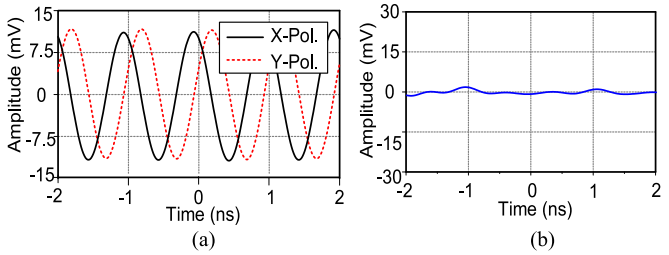

Fig. 8. Waveforms of the IF signals output from (a) PD1 and PD2, and (b) the proposed IRM when the unwanted image is applied.

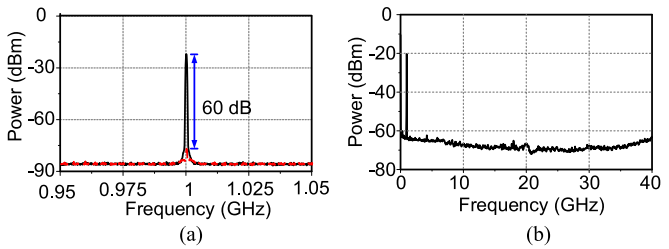

Fig. 9. Electrical spectra of the IF signals downconverted from the useful RF signal (solid line) and the image (dashed line) within the frequency span of (a)100 MHz and (b) 40 GHz.

from the *Y*-polarized branch is shifted by 180°, which agrees well with Eq. (7) in Section II. Fig. 8(b) presents the waveform of the IF signal output from the proposed IRM when the two signals in Fig. 8(a) are combined by the same electrical 90° hybrid. As can be seen, the amplitude of the waveform is nearly zero.

The electrical spectra of the IF signals downconverted from the 20 GHz RF signal and the 19 GHz image are depicted in Fig. 9(a). As can be seen, the power of the IF signal downconverted from the unwanted 20-GHz RF signal (the solid line) is about –20 dBm. Taking the parameters in Table I to Eq. (8), we can calculate that the power of the obtained IF signal is about –18 dBm. Considering that the insertion losses of the optical connectors which is not listed in Table I, the experimental result agrees with the theoretical calculation. On the other hand, the IF signal downconverted from the unwanted 19-GHz image (the dashed line) is below –80 dBm. As a result, an image suppression ratio of more than 60 dB is successfully achieved. The image-reject ratio of the proposed IRM is much larger than the commercially-available electrical IRM, which is typically around 30 dB [22]. To show the mixing spurs suppression performance, an electrical spectrum within the full-span frequency range (0–40 GHz)

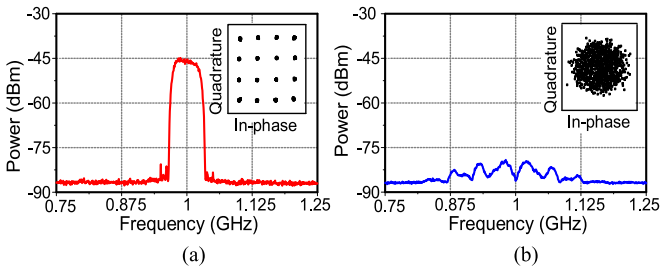

Fig. 10. Spectra of IF signals carrying 50-Mbaud QAM downconverted from (a) the useful RF signal, and (b) the image. (Inset: constellation diagram of the demodulated QAM signal).

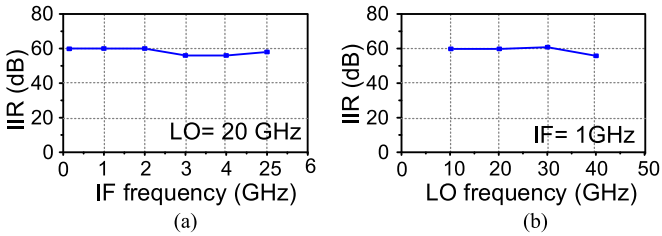

Fig. 11. Image-reject ratio versus the frequency of (a) the output IF signal when the LO frequency is fixed at 20 GHz and (b) the input LO signal when the IF frequency is fixed at 1 GHz. IRR: Image-reject ratio.

of the electrical spectrum analyser is measured and presented in Fig. 9(b). Obviously, only the IF component could be observed within the 40-GHz span, indicating that the mixing spurs have been significantly suppressed.

Then, a 21-GHz RF signal carrying a 50-MBd 16-quadrature-amplitude-modulation (QAM) data is served as the RF signal applied to the proposed IRM. The spectrum of the IF signal downconverted by the proposed IRM is shown in Fig. 10(a), and the corresponding constellation diagram of the demodulated 16-QAM signal is shown as the inset in Fig. 10(a). The error vector magnitude evaluated by 1000 symbols is lower than 2.0%, which shows a good frequency conversion performance of the proposed IRM. Fig. 10(b) shows the electrical spectrum of the downconverted IF signal when the carrier frequency is changed to be the image frequency. The constellation diagram of the demodulated 16-QAM signal is also shown as the inset in Fig. 10(b). As can be seen, the data signal is highly suppressed, indicating that wideband image rejection is realized.

To investigate the performance of the proposed IRM working at different frequencies, the frequencies of the RF and LO signals are changed. Fig. 11(a) shows the image-reject ratio versus the frequency of the output IF signals, when the LO frequency is fixed at 20 GHz and the RF frequency is tuned from 20–25 GHz. As can be seen from Fig. 11(a), image-reject ratio around 60 dB is achieved. Fig. 11(b) shows the image-reject ratio when the LO signal is changed from 10–40 GHz and the IF frequency is fixed at 1 GHz. Again, high image-reject ratio is realized at all these frequencies, demonstrating that the bandwidth of the proposed IRM is large.

The conversion efficiency of the proposed IRM is about −20 dB. Since only the two useful +first-order sidebands are selected by the OBPF, an effective optical amplification can be realized by increase the gain of the EDFA, leading to an improved conversion efficiency [5].

The performance of the optical filters would affect not only the suppression of mixing spurs but also the bandwidth of the proposed IRM. The lower-limit of the RF/LO bandwidth of the proposed IRM is related to the roll-off slope of the optical filters [21], and the upper-limit is dependent on the bandwidths of the modulator and PDs. In the proposed IRM, the operational bandwidth is about 10–40 GHz, since the roll-off factor of the OBPF is about 500 dB/nm [21].

IV. Conclusion

In this paper, we have proposed and demonstrated a novel photonic IRM based on a photonic microwave phase shifter using a DPol-DMZM and an OBPF. A theoretical analysis was performed and a proof-of-concept experiment was carried out. A microwave phase shifter with a tuning range of 0–360° was first realized by adjusting the bias voltage applied to the DPol-DMZM, then, by precisely setting the phase shift of the photonic microwave phase shifter, an IRM with an image-reject ratio of ∼60 dB was achieved when the RF/LO frequency was within 10–40 GHz. In addition, since only the two useful + first-order sidebands were selected by the OBPF before sending to the PDs, the unwanted mixing spurs were suppressed below the noise. The proposed mixer can find applications in future broadband and multifunctional microwave photonic systems.

References

[1] G. K. Gopalakrishnan, W. K. Burns, and C. H. Bulmer, "Microwave-optical mixing in $LiNbO_3$ modulators," *IEEE Trans. Microw. Theory Tech.*, vol. 41, no. 12, pp. 2383–2391, Dec. 1993.
[2] M. E. Manka, "Microwave photonics for electronic warfare applications," in *Proc. Int. Topical Meeting Microw. Photon./Asia-Pac. Microw. Photon. Conf.*, 2008, pp. 275–278.
[3] B. Benazet, M. Sotom, M. Maignan, and J. Perdigues "Microwave photonics cross-connect repeater for telecommunication satellites," *Proc. SPIE*, vol. 6194, 2006, Art. no. 619403.
[4] S. L. Pan, D. Zhu, S. F. Liu, K. Xu, Y. T. Dai, T. L. Wang, J. G. Liu, N. H. Zhu, Y. Xue, and N. J Liu, "Satellite payloads pay off," *IEEE Microw. Mag.*, vol. 16, no. 8, pp. 61–73, Sep. 2015.
[5] E. H. W. Chan and R. A. Minasian, "Microwave photonic downconverter with high conversion efficiency," *J. Lightw. Technol.*, vol. 30, no. 23, pp. 3580–3585, Dec. 2012.
[6] C. Bohemond, T. Rampone, and A. Sharaiha, "Performances of a photonic microwave mixer based on cross-gain modulation in a semiconductor optical amplifier," *J. Lightw. Technol.*, vol. 29, no. 16, pp. 2402–2409, Aug. 2011.
[7] S. N. Fu, W. D. Zhong, P. Shum, Y. J. Wen, and M. Tang, "Simultaneous multichannel photonic up-conversion based on nonlinear polarization rotation of an SOA for radio-over-fiber systems," *IEEE Photon. Technol. Lett.*, vol. 21, no. 9, pp. 563–565, May 2009.
[8] V. R. Pagán, B. M. Haas, and T. Murphy, "Linearized electrooptic microwave downconversion using phase modulation and optical filtering," *Opt. Exp.*, vol. 19, no. 2, pp. 883–895, Jan. 2011.
[9] A. Altaqui, E. H. Chan, and R. A. Minasian, "Microwave photonic mixer with high spurious-free dynamic range," *Appl. Opt.*, vol. 53, no. 17, pp. 3687–3695, Jun. 2014.
[10] S. J. Strutz and K. J. Williams, "A 0.8–8.8-GHz image rejection microwave photonic downconverter," *IEEE Photon. Technol. Lett.*, vol. 12, no. 10, pp. 1376–1378, Oct. 2000.
[11] S. J. Strutz and K. J. Williams, "An 8–18-GHz all-optical microwave downconverter with channelization," *IEEE Trans. Microw. Theory Tech.*, vol. 49, no. 10, pp. 1992–1995, Oct. 2001.
[12] H. Ogawa and H. Kamitsuna, "Fiber optic microwave links using balanced laser harmonic generation, and balanced/image cancellation laser

mixing," *IEEE Trans. Microw. Theory Tech.*, vol. 40, no. 12, pp. 2278–2284, Dec. 1992.
[13] L. Chao, C. Wenyue, and J. F. Shiang, "Photonic mixers and image-rejection mixers for optical SCM systems," *IEEE Trans. Microw. Theory Tech.*, vol. 45, no. 8, pp. 1478–1480, Aug. 1997.
[14] B. C. Henderson and J. A. Cook, "Image-reject and single-sideband mixers," Watkins-Johnson Co., Palo Alto, CA, USA, Tech-Notes, 1985.
[15] Z. Z. Tang and S. Pan, "Microwave photonic mixer with suppression of mixing spurs," in *Proc. 14th Int. Conf. Opt. Commun. Netw.*, Jul. 2015, pp. 1–3.
[16] Z. Z. Tang, F. Z. Zhang, D. Zhu, X. H. Zou, and S. Pan, "A photonic frequency downconverter based on a single dual-drive Mach–Zehnder modulator," in *Proc. Int. Topical Meeting Microw. Photon.*, Oct. 2013, pp. 150–153.
[17] Z. Z. Tang and S. Pan, " A filter-free photonic microwave single sideband mixer," *IEEE Microw. Wireless Compon. lett.*, vol. 26, no. 1, pp. 67–69, Jan. 2016.
[18] C. Middleton, S. Meredith, R. Peach, and R. DeSalvo, "Photonic-based low phase noise frequency synthesis for RF-to-millimeter wave carriers and wideband RF-to-IF down-conversion," in *Proc. Mil. Commun. Conf.,* Nov. 2011, pp. 51–54.
[19] Z. Z. Tang and S. Pan, "A reconfigurable photonic microwave mixer," in *Proc. Int. Topical Meeting Microw. Photon.,* Oct. 2014, pp. 343–345.
[20] Z. Z Tang and S. Pan, "A microwave photonic system for simultaneous frequency mixing and phase shifting," in *Proc. Int. Topical Meeting Microw. Photon.*, Oct. 2015, pp. 1–4.
[21] Z. Z. Tang, S. L. Pan, and J. Yao, "A high resolution optical vector network analyzer based on a wideband and wavelength-tunable optical single-sideband modulator," *Opt. Exp.*, vol. 20, no. 6, pp. 6555–6560, Mar. 2012.
[22] Marki. (2010). IRW-0618 Image Reject Mixer, [Online]. Available: http://www.markimicrowave.com/Mixers/Image_Reject_and_Single_Sideband/Ima ge_Reject/IRW-0618.aspx

Zhengzhou Tang received the M.S. degree in information engineering from the Nanjing University of Aeronautics and Astronautics, Nanjing, China, in 2015. He is currently working toward the Ph.D. degree at the Key Laboratory of Radar Imaging and Microwave Photonics, Nanjing University of Aeronautics and Astronautics, Ministry of Education. His research interests include photonic generation of microwave signals and microwave photonic mixing. He has authored more than 20 research papers, including more than ten papers in peer-reviewed journals and ten papers in conference proceedings.

Shilong Pan (S'06–M'09–SM'13) received the B.S. and Ph.D. degrees in electronics engineering from Tsinghua University, Beijing, China, in 2004 and 2008, respectively. From 2008 to 2010, he was a "Vision 2010" Postdoctoral Research Fellow in the Microwave Photonics Research Laboratory, University of Ottawa, Ottawa, ON, Canada. He joined the College of Electronic and Information Engineering, Nanjing University of Aeronautics and Astronautics, Nanjing, China, in 2010, where he is currently a Full Professor and the Executive Director of the Key Laboratory of Radar Imaging and Microwave Photonics, Nanjing University of Aeronautics And Astronautics, Ministry of Education.

His research interests include on microwave photonics, which includes optical generation and processing of microwave signals, ultrawideband over fiber, photonic microwave measurement, and integrated microwave photonics. He has authored more than 230 research papers, including more than 120 papers in peer-reviewed journals and 110 papers in conference proceedings.

Prof. Pan is a Senior Member of the IEEE Microwave Theory and Techniques Society, the IEEE Photonics Society and a Member of the Optical Society of America. He was selected to receive an OSA Outstanding Reviewer Award in 2015. He is the Chair of numerous international conferences and workshops, including the TPC Chair of the International Conference on Optical Communications and Networks in 2015, the TPC Chair of the high-speed and broadband wireless technologies subcommittee of the IEEE Radio Wireless Symposium in 2013, 2014, and 2016, the TPC Chair of the Optical fiber sensors and the microwave photonics subcommittee chair of the OptoElectronics and Communication Conference in 2015, and the Chair of the microwave photonics for broadband measurement workshop of International Microwave Symposium in 2015.